NTNU – Trondheim
Norwegian University of
Science and Technology

The Influence of the Energy Degrader Material for a Therapeutical Proton Beam

John Alfred Brennsæter

The Influence of the Energy Degrader Material for a Therapeutical Proton Beam

John Alfred Brennsæter

June 2015

Department of Physics

Norwegian University of Science and Technology

Supervisor: Associate Professor Pål Erik Goa

Abstract

In cyclotron based proton therapy an energy degrader is needed to modulate the proton beam energy. The proton beam energy decides the range of the particles and thereby where the dose is imparted. The influence of the material of the energy degrader for a 250 MeV therapeutic proton beam has been evaluated with FLUKA, a Monte Carlo based particle transport software. A geometry of a double wedge degrader of beryllium, carbon or lexan and a collimator of copper and carbon has been used. The momentum spread, angular spread, transmission fraction neutron yield and photon yield have been measured. The results show that the momentum spread is unaffected of the degrader material. The momentum spread affects the transmission fraction as the maximum momentum spread has to be limited by a momentum slit after the degrader. In the next round this also leads to that the distal dose fall off in a compact proton therapy facility without a momentum analyzer is unaffected by the degrader material. Further, the results have shown that beryllium gives a lower angular spread than the other materials. The transmission fraction through the degrader and collimator is around 2% for all degrader materials at 70 MeV. Due to the reduced angular spread a beryllium degrader may increase the transmission fraction with as much as 43% for short range degraded proton beams compared to a carbon degrader. Beryllium has also shown to generate the highest amount of neutrons. For a 70 MeV proton beam, the neutron yield is increased with 50% compared to a carbon degrader, and with 82% compared to a lexan degrader. This leads to extended harmful neutron radiation that increases the need for neutron shielding around the degrader. This makes beryl-

lium a less attractive degrader material for a compact proton therapy facility, as the degrader then is located close to the treatment room.

Sammendrag

I syklotronbasert protonterapy er man avhengig av å benytte en energi-modulator for å modulere energien til protonene. Energien til protonene bestemmer hvor langt inn i vevet partiklene beveger seg før de stopper, og dermed hvor dosen blir avsatt. Påvirkningen energimodulatormateri-alet har på en 250 MeV terapeutisk protonstråle har blitt studert med det Monte Carlo baserte partikkelsimuleringsprogrammet FLUKA. Et oppsett med to motstående kiler av beryllium, karbon eller lexan og en kollima-tor bestående av kobber og karbon har blitt brukt. Spredningen i beveg-elsesmengde og vinkelspredning, samt transmisjonsfraksjon og produk-sjon av nøytroner og fotoner har blitt målt. Resultatene viser at det ikke har noen innvirkning på spredningen i bevegelsesmengde blant protonene som ble modulert hvilkett materiale modulatoren består av. Spredning-en i bevegelsesmengde påvirker den totale transmisjonsfraksjonen til systmet, siden den maksimale spredningen i bevegelsesmengde må bli redusert av en bevegelsesmengdeanalysator etter modulatoren. Siden spredningen i bevegelsesmengde er konstant for alle materialer, fører dette til at stråledosen avtar like hurtig i bakkant av Bragg-peaken for alle materialer og energier ved samme opprinnelige energi før modulering uten bevegelsesmengdeanalysator. Videre viser resultatene at beryllium gir snevrere vinkelspredning enn karbon og lexan. Transmisjonsfraksjo-nen gjennom modulator og kollimator er omtrent 2% når strålen blir modulert ned til 70 MeV. På grunn av den reduserte vinkelspredningen for beryllium kan transmisjonsfraksjonen bli økt med opptil 43% for de laveste energiene sammenlignet med en karbonmodulator. Resultatene viser også at beryllium er det materialet som genererer flest nøytroner.

For en 70 MeV stråle genereres det 50% flere nøytroner i en beryllium modulator enn i en karbon modulator og 82% flere enn i en lexan modulator. Dette fører til økt skadelig nøytronstråling fra modulatoren som øker behove for skjerming. Av den grunn blir beryllium et mindre attraktivt materiale å benytte seg av i et kompakt protonterapisenter, siden modulatoren da ofte er plassert nært behandlingsrommet.

Preface

This master thesis in medical physics at Norwegian University of Science and Technology(NTNU) is part of the study program Biophysics and medical technology. This thesis has been carried out during the spring semester of 2015. The idea to the thesis was brought up by Project Manager Odd Harald Odland at Haukeland University Hospital in cooperation with Associate Professor Pål Erik Goa at NTNU and Professor Dieter Röhrich at the University in Bergen.

The topic for the thesis came up after Odd Harald Odland visited the US in January and observed that the Midwest Proton Radiation Institute at Indiana University utilized a beryllium degrader for energy modulation of the proton beam.

Trondheim, 02.07.2015

John Alfred Brennsæter

Acknowledgment

I would like to thank the following persons for their great help during my master study.

Project Manager Particle Therapy Odd Harald Odland at Department of Oncology and Medical Physics Haukeland University Hospital for professional input and great support during my work with the thesis.

Vladimir Derenchuk and the ProNova solutions for great cooperativeness and useful input for the simulations.

Professor Dieter Röhrich at the Department of Physics University in Bergen for interest and cooperativeness for my work with the thesis.

Kristian Smeland Ytre-Hauge for great help with FLUKA-simulations.

Sigrun Saur Almberg, Jomar Frengen and the Clinic of Oncology St. Olavs Hospital for their supportive interest. A special thank you to Sigrun, who spent some of her precious time to review my thesis. It was really appreciated!

Eivind Rørvik for professional conversations and discussions and cooperation during the project. A special thank you for always showing up so late in the day. It made me feel like I got up early in the morning! I would also like to thank Kjetil Viste Levik and Daniel Wennberg for participating in the suffering the latest days in June and even July.

I would also like to thank my friends and house mates throughout my time in Trondheim. You have made my stay here in this city of mustache to a great time I will remember with gratitude. A special thanks to the two of you who brought me ice cream and strawberries on the final day!

My family also deserves a thank you in this context. Thank you for a good childhood in the woods of Hurdal. I still always look forward to

come home. For vacation. I really appreciate all of you! A special thank you to my grandparents, Reidun and Olav Bergene Holm, for letting me borrow your car for so long time! It was really great to have a car during my life as a student. I am really sorry I crashed it!

Finally, I would like to to thank my supervisor Associate Professor Pål Erik Goa for great support during the entire project. You are a great supervisor I will recommend to all other students.

J.A.B.

Abbreviations

FWHM Full Width Half Maximum

ESS Energy Selection System

SOBP Spread-out Bragg Peak

Contents

Chapter 1

Introduction

After Wilhlem Röntgen's discovery of the X-rays in 1895 [1], radiotherapy has been an important modality in cancer treatment, with photons as the most common type of radiation. Radiation therapy utilizes ionizing radiation, which damages all kinds of cells, with the purpose to kill tumor cells. From Röntgen's discovery in 1895 the techniques for radiation therapy have been continously improved. This has led to better localization of the tumors and better precision of the beam. In 1946 Robert R. Wilson proposed to use high energy protons in radiation therapy [2]. The use of protons and other heavy ions in radiation therapy has increased exponentially during the last few decades. To take advantage of the characteristic depth dose distribution of protons, proton therapy requires accurate localization of the target volume. Image guided radiation therapy and modern beam delivery techniques make it possible to benefit from this potential.

Inevitably, radiation therapy not only damage tumor cells, but also the surrounding healthy tissue. The aim of radiotherapy is to achieve

a high tumor control probability (TCP) at an acceptable normal tissue complications probability(NTCP). Compared to photons, the dose deposition of protons thereby result in a lower dose to the surrounding healthy tissue while maintaining the tumor dose [3].

In proton therapy protons are accelerated either by a cyclotron or a synchrotron. Cyclotron based proton therapy usually utilizes an energy selection system to modulate the beam energy. The energy selection system consists of a degrader and a momentum analyzer. While the degrader modulates the particle energy, the momentum analyzer filters out secondary particles generated in the degrader and protons with too high or too low energy, to make the beam as monoenergetic as desired. The degrader material influences the beam in several ways. Some protons will be scattered and stopped in the collimator behind the degrader, some protons will interact with a nucleus in the degrader and generate secondary particles, some protons will be degraded more than desired and stopped by the momentum slit, and some protons will be degraded to the desired energy and continue towards the treatment room. For the worst cases, less than 1 % of the beam is transmitted through the degrader system [4]. To maintain an acceptable high dose rate it is important to keep the transmission fraction through the degrader and collimator as high as possible. Degraders and collimators are the main soures of secondary neutrons in proton therapy [5]. Due to the long range of neutrons, stray radiation from neutrons is the main shielding reason in proton therapy [6].

The Midwest Proton Radiotherapy Institute, Indiana, USA utilizes a double wedge beryllium degrader [7]. Other possible degrader materi-

als are carbon [8] or plastics, as for example the polycarbonate lexan [9]. The aim of this thesis is to investigate which degrader material that is best suited to modulate a therapeutic proton beam with initial energy 250 MeV. The consequences of degrading a proton beam with a double wedge degrader have been simulated by the Monte Carlo tool FLUKA [10]. Degraders made by beryllium, carbon and lexan were compared. Simulations have been done with and without collimators behind the degrader. The momentum spread and the angular spread of the beams were evaluated and thereby the transmission fraction in the degrader, in addition the difference in neutron and photon yield in the degrader and collimator was evaluated. The main focus in the thesis will be around the beryllium degrader, while carbon and lexan are used for comparison.

The figures presented in this thesis is from work performed by the author unless otherwise is specified.

Chapter 2

Theory

2.1   Interactions between protons and matter

Protons traversing matter interact with nuclei and electrons in the material. There are three different ways protons interact with matter; stopping due to coloumb interactions with electrons, scattering due to coloumb interactions with nuclei, and nuclear interactions due to inelastic collisions with nuclei. The theory chapter in this thesis is roughly based upon Proton Therapy Physics, edited by Harald Paganetti[5].

2.1.1   Stopping

Stopping is caused by electrostatic interactions between protons and atomic electrons. As the proton mass is about 2000 times higher than the electron mass, the direction of the protons is not much influenced by these interactions. The amount of energy transfered in an event of an interaction between an incoming proton and an electron is related to the time

Table 2.1: Terms in the Bethe formula

Abbreviations
r_e: classical electron radius
m_e: electron mass
N_a: Avogadro's number
I: Mean excitation potential
Z: atomic number of absorbing material
A: atomic weight of absorbing material
ρ : Density of absorbing material
z: charge of incident particle in units of e
β: v/c of the incident particle
$\gamma : \frac{1}{\sqrt{1-\beta^2}}$
δ : density correction
C: shell correction
W_{max}: Maximum energy transfer in a collision

the proton is in the electrons vicinity. This leads to a characteristic increase in energy transfer in the final stage, when the proton stops. This is known as the Bragg peak for heavy charged particles. The relation between the deposited dose and particle fluence(see section 2.5) is shown in figure 2.1. The stopping power of a material is defined by the Bethe-Bloch formula for heavy charged particles (Equation 2.1) [11], where the terms are defined in table 2.1.

$$S = -\frac{dE}{dl} = 2\pi N_a r_e^2 m_e c^2 \rho \frac{Z}{A} z^2 \beta^2 \left(\ln \frac{2 m_e v^2 \gamma^2 W_{max}}{I^2} - 2\beta^2 - \delta - 2\frac{C}{Z} \right)$$

$$(2.1)$$

The mass stopping power is in many cases a more convenient parameter. It is defined as $\frac{S}{\rho}$ where ρ is the density of the stopping material.
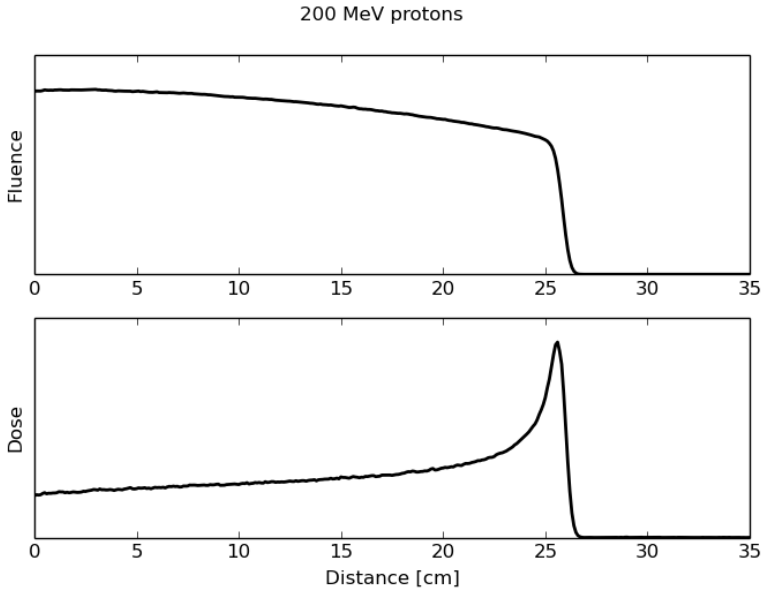
Figure 2.1: Monte Carlo simulations of the connection between proton fluence(see section 2.4) and dose deposition for a 200 MeV proton beam in water

2.1.2 Scattering

Scattering is caused by electrostatic elastic interactions between protons and atomic nuclei. While traversing through the matter, the protons will be scattered multiple times. Hence, the total scattering through a material is a sum of many interactions which gives an almost gaussian distribution [5]. Highland's formula (Equation 2.2) is a gaussian approximation of the root mean square scattering angle

$$\theta_0 = \frac{14.1 MeV}{pv} \sqrt{\frac{L}{L_R}} \left(1 + \frac{1}{9} log_{10}\left[\frac{L}{L_R}\right]\right) \tag{2.2}$$

, where p and v is the momentum and the velocity of the paprticle respectively, L is the length of the material the particle is traversing and L_R

is the radiation length of the material.

2.1.3   Nuclear Interactions

Nuclear interactions is caused by inelastic collisions between the incoming proton and atomic nuclei causing a nuclear reaction. Protons enter the nucleus and interact with it, and another particle is emitted. The emitted particle can be a proton, neutron or a cluster of nucleons. These are called secondary particles. The local effect of the generation of secondary particles is small [5]. However, the secondary particles move on and will transfer their energy over a large distance. While the elastic scattering of protons typically change the direction with only a few degrees, the secondary particles can make a large angle with respect to the beam [5]. For low energy protons, the electrostatic repulsion between the proton and the nucleon prevents nuclear interactions from happening, but this is negligable for proton energies much larger than 100 keV [12].

2.2   Interactions between neutrons and matter

Due to nuclear interactions from protons, neutrons are generated in both tissue and aperture in the beamline. While protons and other charged particles react strongly with matter, neutrons are significantly less reactive. Neutrons have no charge and have therefore no electromagnetic interaction with neither the electrons nor the nuclei. They can travel a much longer distance than protons and other charged particles. A comparison of the range of 200 MeV neutrons and protons are shown in figure 2.2. Neutrons with different energies interact differently. The different
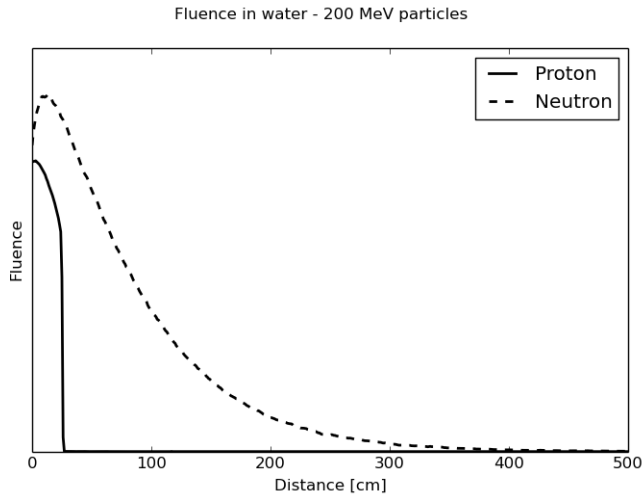
Figure 2.2: Monte Carlo simulations of 200 MeV protons and neutrons in water. All protons have stopped after 26 cm, while the attenuation length of the neutrons is 115 cm. Some neutrons are even traversing more than 300 cm.

Table 2.2: Neutron energy classification [5]

Class	Energy range
Thermal	$E_n < 0.5$ eV
Intermediate	0.5 eV $< E_n < 10$ keV
Fast	10 kev $< E_n < 20$ MeV
Relativistic	$E_n > 20$ MeV
High-energy	$E_n > 100$ MeV

neutron classes are shown in table 2.2.

Neutrons interact with matter when they collide with other nuclei. This can be either an inelastic or elastic reaction. For the elastic reactions the kinetic energy is conserved, but for the inelastic reactions the nucleus is left in an excited state after the collision with a neutron. Hence, the inelastic scattering threshold equals the lowest excited state of the material. A neutron can also be captured in reactions like (n,γ), (n,2n) and several other reactions [5].

2.2.1   Relativistic neutrons

Neutrons with energies above 50 MeV regenerates lower energy neutrons by nuclear reactions. Neutrons can interact with a single nucleon in the nucleus and thereby evaporate other particles from the nucleus. When there is no more energy left for particle emission, the rest of the excitation energy is released as a gamma ray. However, the nucleus may still be radioactive if the nucleus is an unstable isotope.

2.2.2   Fast neutrons

Fast neutrons may also regenerate more neutrons. Their energy is reduced by several elastic and inelastic reactions, until it is reduced to intermediate and then thermal neutrons or undergo radiative capture. As the energy decreases the probability for inelastic reactions decreases. Inelastic reactions dominates for energies above 10 MeV, while there is almost only elastic scattering for neutron energies below 1 MeV[5].

2.2.3   Thermal neutrons

The neutrons with lowest energy are called thermal neutrons. The name is based on the fact that they are in approximate thermal equilibrium with the surrounding particles. Thermal neutrons are scattered by elastic scattering, because they do not have enough energy to excite other nuclei. They diffuse about, until they eventually undergo radiative capture.

2.2.4 Neutron shielding

Due to neutron's long range, extra precautions have to be taken to protect the surroundings from harmful radiation. Most proton therapy facilities therefore place elements that interact with the protons as far away from the treatment room as reasonably achievable. This makes it possible to shield the patients and staff from unwanted secondary radiation. Neutron shielding consists of a mixture of high Z materials to reduce the neutron flux of high energy neutrons through inelastic scattering and low Z materials to reduce the low energy neutrons through elastic scattering [13]. Finally, the neutrons are captured preferably by absorbers, typically boron or lithium.

2.3 Interactions between photons and matter

Due to nuclear interactions, photons are also generated in both tissue and aperture during proton irradiation. After a nuclear interaction the nucleus may be left in an excited state. This results in an emitted photon when the nucleus returns to the ground state. In the MeV range photons interact with matter in mainly three different ways; photoelectric effect, compton scattering and pair production[14]. The attenuation coefficients for the different interactions are shown in figure 2.3.

2.3.1 Photoelectric effect

A photon may interact with an orbital electron of an absorber atom. In photoelectric effect, the photon transfers all its energy to the electron,
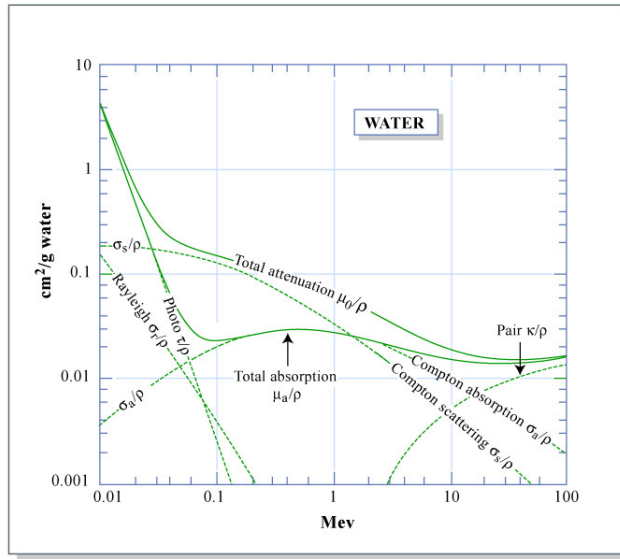
Figure 2.3: Mass attenuation coefficients for photons in water. Figure by MIT OpenCourseWare.

which is kicked out from the atom it is bound to. A new characeristic x-ray photon for the atom is emitted due to an electron filling the vacancy from the released electron. Photoelectric effect is most common for high Z materials and for energies below 100 keV.

2.3.2   Compton scattering

When a photon interacts with an orbital elctron, it may also transfer parts of its energy. Hence, the photon is scattered an angle θ and the momentum of the electron is decided by conservation of momentum from the photon.

2.3.3 Pair production

When a photon has higher energy than 1.022 MeV it may interact near a nucleus in a process called pair production. The photon disappears and reappear as a positron and an electron. The limit of 1.022 MeV is due to the rest energy of the electron and the positron which is 511 keV.

2.4 Dose Deposition

As protons traverse through matter, energy is deposited to the matter. The dose is defined as the energy imparted per unit mass:

$$D \equiv \frac{E}{m} \tag{2.3}$$

The particle fluence Φ is defined as the number of particles that intersect a unit area.

$$\Phi \equiv \frac{dN}{dA} \tag{2.4}$$

If dN particles passes through a cylinder with surface dA and thickness dl, the dose can be written:

$$D = \frac{E}{m} = \frac{-(dE/dl) \cdot dl \cdot dN}{\rho \cdot dA \cdot dl} = \frac{dN \cdot S}{dA \cdot \rho} \equiv \Phi \frac{S}{\rho} \tag{2.5}$$

This shows the relation between particle fluence and dose.

For radiation therapy, the purpose is to deposit as much as possible of the dose within the target volume. Hence, the distal dose distribution for protons is advantageous, due to the low entrance dose and the
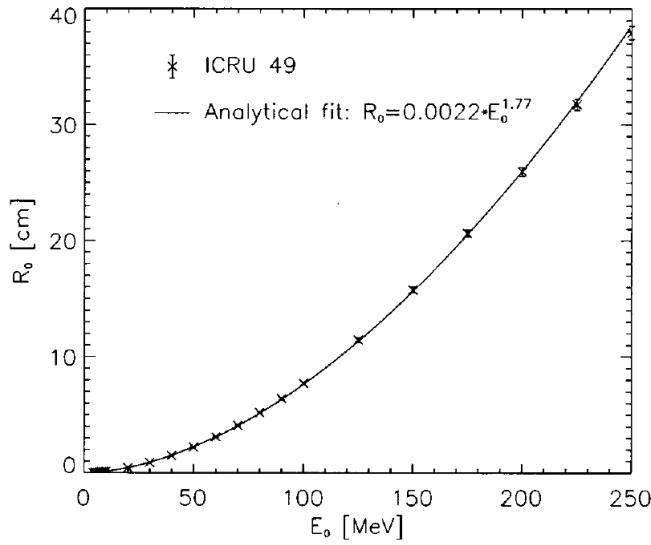
Figure 2.4: The mean projected range in water for protons with various initial energy. [15].

total absence of dose behind the Bragg peak. In order to cover the entire target volume with a homogenous dose, the entrance energy is varied and thereby making a so called "Spread out Bragg-peak" - SOBP. This may give a significantly lower dose to normal tissue surrounding the target volume compared to photon therapy[3], even though photon therapy benefits from more mature technology.

2.5 Range

The range of a proton is strongly related to the initial kinetic energy, as shown in figure 2.4. The kinetic energy and the momentum of the protons are often used interchangeably and is indeed equivalent as $E = \frac{p^2}{2m}$. International Commission on Radiation Units & Measurements (ICRU) have given experimental results for proton range in water that fits to

$$R_0 = \alpha E_0^p = 0.0022 E_0^{1.77} \qquad (2.6)$$

where E_0 is given in MeV and R_0 in cm[15]. The mean projected range, R_0, of a proton beam is defined as the range where half of the protons that do not undergo nuclear reactions have stopped. This corresponds with the distal 80% of the Bragg peak, d_{80} [16]. Due to historic reasons the range of a proton beam is often referred to as the distal 90% of the dose. As shown in figure 2.1 all protons that do not undergo nuclear interactions stop over a short region. This attribute ensure that there is almost no dose deposited to the region behind the target volume. Due to the relation between energy and range, it is important to have a narrow energy spectrum to benefit from the characteristic depth dose distribution of protons. However, even with an extremely narrow energy spectrum there will be some range straggling due to different scattering in the tissue. All particles will traverse slightly different, which gives a little variation in range.

2.6 Momentum spread

As the range of the particles and thereby the range of the Bragg peak is strongly related to the momentum of the proton, it is important to make sure that the beam has a low momentum spread. An increased momentum spread leads to a broader Bragg peak, which again leads to an increased distal dose fall off. The distal dose fall-off is also known as the distal penumbra. Clinically it is beneficial to keep the distal penumbra as short as possible to spare normal tissue behind the target volume. How
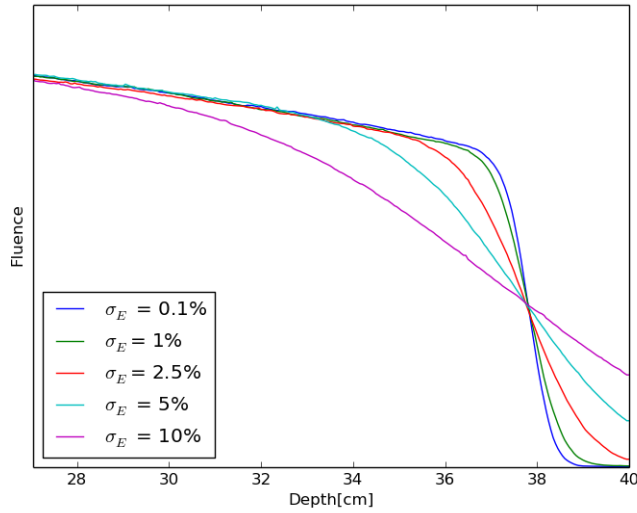
Figure 2.5: Monte Carlo simulations of proton fluence in water for 250 MeV proton beam with different momentum spread.

the momentum spread affects the proton fluence is shown in figure 2.5

2.7   Transmission fraction

The transmission fraction, T, of an element in the beam line tells how much the beam intensity has been reduced after going through the element.

$$T = \frac{I}{I_0} \tag{2.7}$$

In order to maintain a sufficiently high dose rate it is important to keep the transmission fraction as high as possible.

2.8   Particle accelerators

In proton therapy protons are usually accelerated by either a cyclotron or a synchrotron. A cyclotron is accelerating the protons in a constant magnetic field by a varying electric field. The protons follows a spiral path until they reach the velocity that make them escape from the magnetic field into the beam line. A synchrotron is accelerating protons following a constant path. The protons are accelerated by a linear accelerator and bending magnets turns the beam around and through the linear accelerator several times, until the protons have the desired energy and another magnet leads them in to the beam line. Due to these properties of the accelerators, a synchrotron may only deliver protons in pulses, while a cyclotron delivers a continuous beam[17]. The synchrotron is also generally more space consuming and demands higher operating costs than cyclotrons[18]. The synchrotron has the advantage that it is possible to choose the wanted energy directly, while the cyclotron can only deliver protons at one predetermined energy. Due to these properties, the cyclotron based proton therapy facilites needs an energy degrader to adjust the proton energy to make the SOBP at the wanted depth.

2.9   Energy Selection System

Due to the cyclotron's lack of ability to select proton energy, there is a need for an energy selection system (ESS). The most important components of an ESS is an energy degrader, collimators and focusing and bending magnets (see figure 2.6. The degrader slows down the protons to the wanted energy level. A collimator stops the protons which have
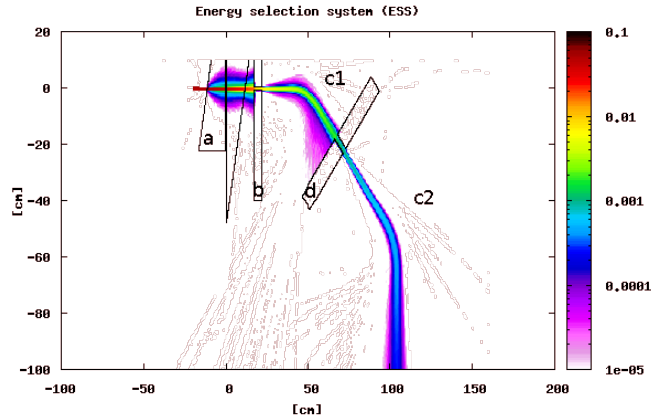
Figure 2.6: Monte Carlo simulation of the principle of an ESS with degrader(a), collimator(b), bending magnets(c1, c2) and momentum slit (d). A 250 MeV proton beam is degraded to 70 MeV. The simulations do not include focusing magnets which lead to somewhat higher beam loss and angular spread.

been scattered in the degrader. Quadropole magnets focuses the beam, before dipole magnets bends the beam. A momentum slit lets the protons with momentum in the desired interval through, based on the beam direction after the bending magnets. All particles with undesired energy will be bent differently and be stopped by the momentum slit, which is basicly a collimator. This leads to a significant loss of protons. Typically, an ESS has a transmission fraction at around 1 %for the lowest beam energies[19].

2.9.1   Energy Degrader

The energy degrader is slowing down the protons to the wanted energy level. The energy degrader is basically a material with adjustable thick-
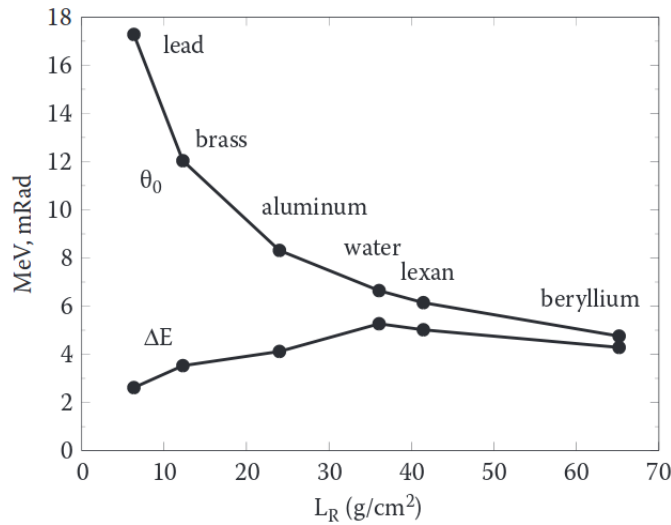
Figure 2.7: Multiple scattering angle and energy loss for a 160 MeV proton beam traversing 1 g/cm^2 of various materials. [5]

ness placed in the beam line after the accelerator. In order to maintain as high beam intensity as possible the transmission fraction through the degrader should be as high as possible. It is therefore desireable to have a minimum of scattering with nuclei and nuclear interactions in the degrader. Scattering is unfavorable, because it leads to particles being stopped in the collimators after the degrader. Nuclear interactions are unfavorable, because it leads to both loss of protons in the beam and also generates possible harmful secondary radiation. Due to the generation of secondary particles, the degrader should be placed well shielded, far away from the treatment room. Several different materials are beeing used for degradation, for example Beryllium, Carbon and Lexan[9]. Some important properties of these materials is shown in table 2.3.

Table 2.3: Radiation length (L_R) and density for relevant degrader materials[9].

Material	<Z/A>	ρ (g/cm^3)	L_R (g/cm^2)
Beryllium	0.44384	1.848	65.19
Carbon	0.49954	2.265	42.70
Lexan	0.52697	1.20	41.46

2.9.2 Collimators

After the protons have been degraded the beam is collimated. This stops the protons that have been scattered too much in the degrader. However, as some protons interact with the material in the collimator, there will be generated secondary particles in the collimator aswell.

2.9.3 Focusing Magnets

After the collimator the beam is focused by quadrupole magnets. A quadrupole magnet is focusing the beam in one spatial direction, so there have to be two different quadrupole magnets to focus the beam in both directions. There should be quadrupole magnets several places along the beam line to keep the beam focused in both transversal directions.

2.9.4 Bending Magnets

After focusing, the beam goes through a dipole magnet which bends the beam according to the energy of the particles. This leads to protons with different direction based on kinetic energy. It also sorts out different secondary particles that have been generated in the degrader and collimator as they will not be bent the same way as protons. The radius of the curve during bending is given by the Lorentz force which for relativistic veloci-

ties comes out like

$$r = \frac{\gamma m v}{qB} \tag{2.8}$$

where r is the radius, γ is the Lorentz factor, m, v and q is respectively the rest mass, the velocity and the charge of the particle, and B the magnetic B-field.

2.9.5 Momentum slit

After the beam is bended, there is a momentum slit, which is a kind of a collimator, that lets the particles with momentum in the desired interval through. This interval may vary somewhat for different beam lines. At the Paul Scherrer Institut (PSI) in Switzerland the maximum momentum spread is ±1.2% of the mean energy of the degraded beam[20].

Chapter 3

Methods

The Monte Carlo simulations in this project have been performed with FLUKA v. 2011.2c.0 [10] and a graphical interface software, Flair v. 2.1-1 [21]. The FLUKA code has shown to be a suitable choice for simulations in proton therapy [22] The initial beam was a gaussian shaped 250 ± 2.3 MeV proton beam, which secures a momentum spread below 1% of the mean energy [5], with spatial FWHM of 0.25cm in both transversal directions. The beam was initialized in x=-20cm, y=0cm, z=0cm and directed towards the degrader, which was centered around origo, see figure 3.1. Three different materials were used to modulate the beam energy, beryllium, carbon and the polycarbonate Lexan. For each simulation 10^5 primary particles were initialized to give the simulations satisfactory statistics within reasonable simulation time. There have been done simulations both with and without a collimator after the degrader.

3.1 Geometry of the ESS

The geometry of the FLUKA setup consists of a double wedge degrader
and a water phantom. The degrader is placed in a vacuum sphere, which
makes it possible to score the secondary particles that crosses the bound-
ary of the sphere. The water phantom is also placed in vacuum so the
proton beam does only traverse through vacuum until it hits the water
phantom. In the simulations with a collimator, the collimator has been
placed within the vacuum sphere with the degrader. This makes it possi-
ble to score the secondary particles that have been generated in both the
degrader and the collimator.

3.1.1 Degrader

The energy degrader in this project is based on a double wedge system
as shown in figure 3.2. The wedges have been kept symetrical around
the beam axes for all energy degradations by adjusting both wedges si-
multaneously. Each wedge is 70cm long, 20 cm wide and 16.471 cm deep
and seperated by a 0.4 cm gap. This gives the wedge a slope of 13.2°.
The dimensions of the degrader is based on the double wedge beryllium
degrader produced by ProNova. This geometry ensures that the system
is able to degrade a proton beam from 250 MeV to 70 MeV with either
beryllium, carbon or lexan.

3.1.2 Collimator

A collimator has been simulated by a 6.5 cm deep copper cylinder with
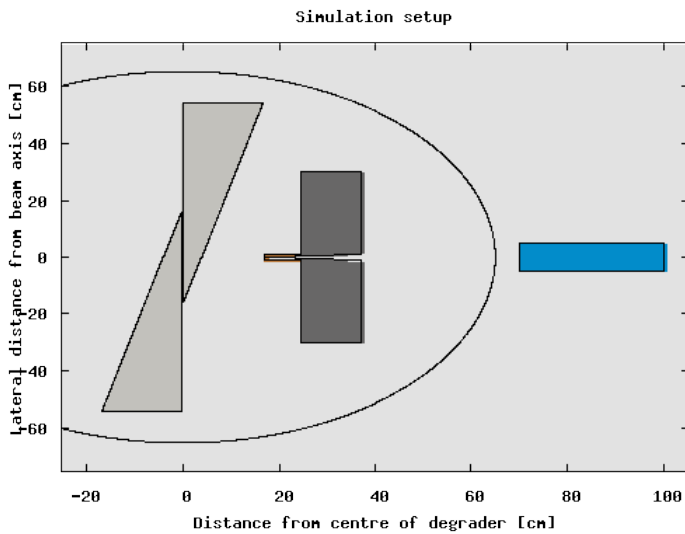radius of 1.3 cm with a cone shaped collimator hole with radius of 0.35

Figure 3.1: Setup for the simulations with collimator. The degrader is positioned around x=0, followed by a tiny copper collimator and a bigger Carbon collimator. All elements are placed inside a spherical region which makes it possible to score total number of neutrons and photons generated in the degrader and collimators. Finally, the beam enters a water phantom. All elements are surrounded by vacuum.
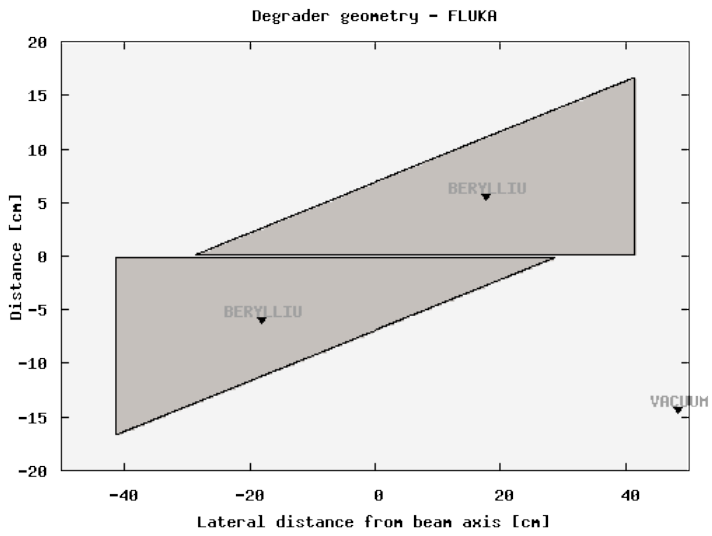
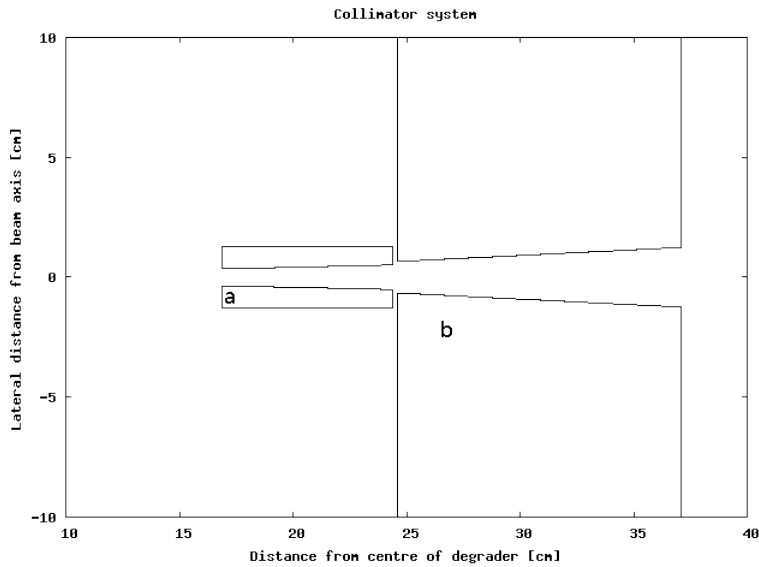Figure 3.2: Beryllium degrader geometry for modulating a 250 MeV proton beam to 160 MeV.

Figure 3.3: Collimator geometry for the simulations done in this work. (a) is the Copper collimator that limits the beam and (b) is the Carbon collimator that stops the protons that is scattered past (a).

cm at the degrader side and 0.514 cm at the far side placed 0.2 cm behind the far edge of the degrader. 0.23 cm behind the copper collimator is a carbon collimator with an outer radius of 30 cm with a cone shaped collimator hole with a radius of 0.65 cm closest to the degrader and 1.25 cm at the far side. The collimator setup is based on the collimator in PSI, Willigen[4]. The copper collimator is as small as possible to reduce activation of the collimator, while the carbon collimator stops protons that is scattered past the copper collimator.

3.2 Scoring

The scoring of the different properties is in FLUKA done with different scoring cards.

3.2.1   Momentum spread

The energy spectrum has been scored with the USRBDX card[10], which scored the proton fluence of the protons entering the water phantom for an energy interval of 20 MeV around the mean energy with a resolution of 200 bins. The USRBDX card scores the kinetic energy of particles crossing a boundary between two regions. In addition to the energy spectrum, the transmission fraction of the beam has been measured with the same card. Based on the energy spectrum, the number of particles within a momentum spread threshold of 1.2 % has been measured. The threshold used here is based on the momentum analyzing system at PSI[20].

3.2.2   Angular spread

The angular spread has been scored in the area between the degrader and the water phantom for the collimated beam with the USRBIN card[10]. The USRBIN card scored the proton fluence for the protons entering the water phantom for all angles around the beam axis with a resolution of 2999 bins. The USRBIN card may score different properties like particle fluence and dose in a specific area, and is well suited for scoring spatial properties. According to Stichelbaut and Jongen the beam divergence of the degraded beam needs to be lower than 12 mrad[23] for an ion beam therapy system. For the uncollimated beam the fraction of the beam that has a lower angular spread than 12 mrad have been calculated based on the angular beam profile.

3.2.3 Distal penumbra

The distal penumbra of the Bragg peak has been measured by scoring the total dose with the USRBIN card. The dose was scored with 1000 bins for 10 cm around the Bragg peak.

3.2.4 Neutron yield

The secondary neutron generation has been scored with the USRBDX card, which scored the fluence of neutrons leaving the ESS. Both the total amount of neutrons and the energy spectra of the neutrons was scored.

3.2.5 Photon yield

The photon production has been scored with the USRBDX card, which scored the fluence of photons leaving the ESS.

Chapter 4

Results

4.1 Uncollimated beam

4.1.1 Degrader thickness

The material thickness needed to modulate the 250 MeV proton beam to the wanted energy level is shown in figure 4.1. A beryllium degrader will decrease the thickness with 24% compared to lexan, but it will also increase the thickness with 18% compared to carbon. The same wedge size have been used in all simulations. However, this results shows that it is possible to use a significantly smaller carbon wedge, compared to lexan.

4.1.2 Momentum spread

The momentum spread of the beam after degradation with different materials is shown in figure 4.2. The FWHM of the spectra is shown in figure 4.3. There are no differences of significance for the different degrader
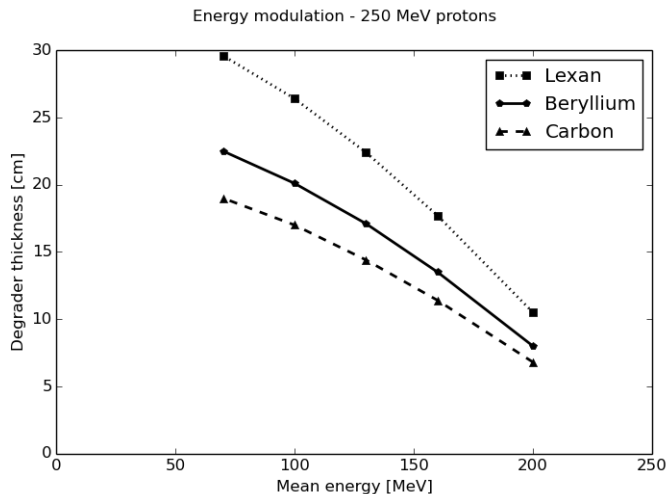
Figure 4.1: Degrader thickness needed to modulate the mean energy of the proton beam to the wanted level. Initial proton energy: 250 MeV.

materials. The momentum spread of the beam increases for increasing energy degradation. Even though there are some differences in the thickness of the degrader for the different materials, this does not affect the momentum spread. The momentum spread does only depend on the initial and final energy.

4.1.3 Distal penumbra

As the momentum spread after the energy degradation is the same for all materials, the distal penumbra for an uncollimated beam is also approximately equal for all degrader materials. This is shown in figure 4.4. The distal penumbra is constant 0.55 - 0.58 cm for all energies and degrader materials.
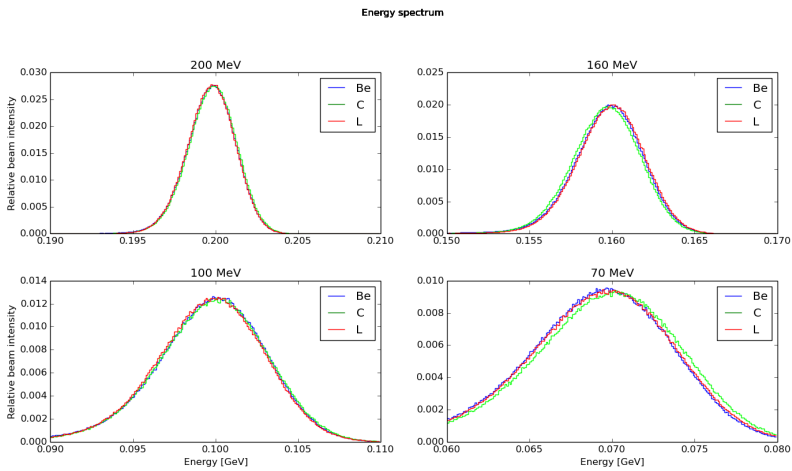
Figure 4.2: Momentum spread for some of the degraded proton beams. The spectra broadens as the protons are degraded more. There is no difference between the different degrader materials. Initial proton energy: 250 MeV.
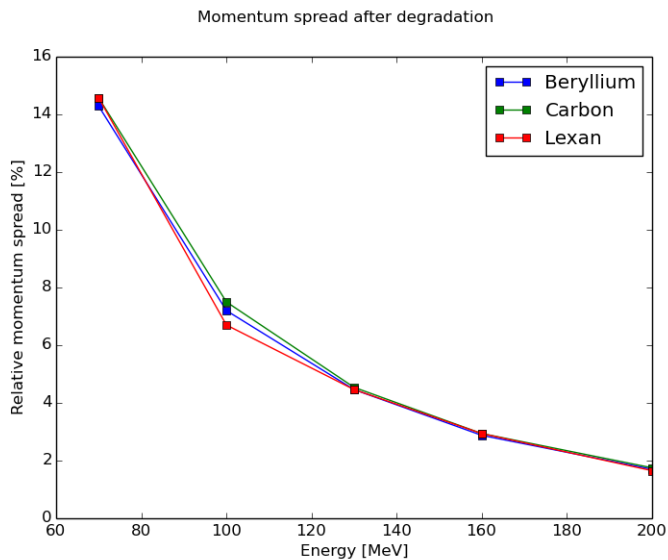

Figure 4.3: The relative full width half maximum of the momentum spread of the proton beam after degradation. Initial proton energy: 250 MeV.
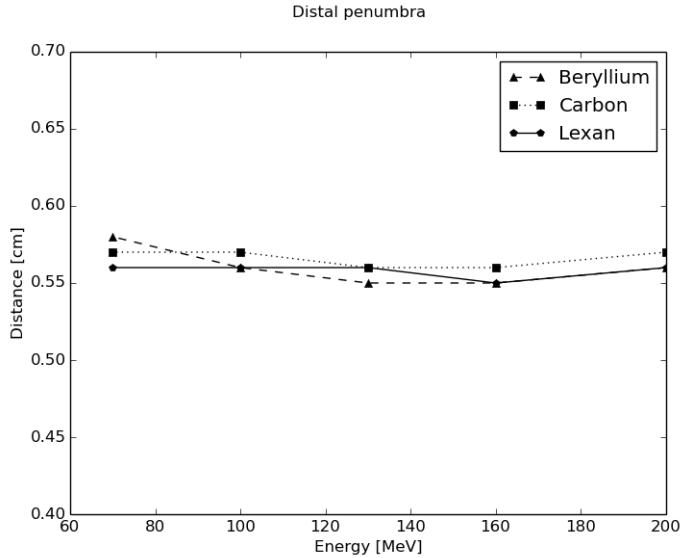
Figure 4.4: The distal penumbra in water for an uncollimated degraded proton beam. Initial proton energy: 250 MeV.

4.1.4   Angular spread

As shown in figure 4.5, the angular beam profile is gaussian shaped. The HWHM has been measured to compare the angular spread of the different degrader materials, as the orientation of the angle shoud be indifferent.

The HWHM of the angular spread of the beam after degradation with different materials is shown in figure 4.6. A beryllium degrader leads to 20% less angular spread than a carbon or lexan degrader.

4.1.5   Transmission fraction

The transmission fraction through the degrader is shown in figure 4.7. When ignoring the angular spread of the beam and only measuring the number of protons transmitted through the degrader, the beryllium de-
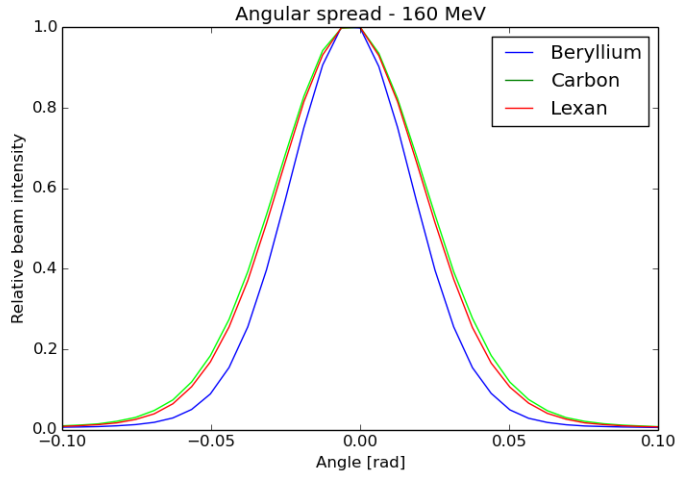
Figure 4.5: Angular beam profile for an uncollimated beam degraded from 250 MeV to 160 MeV.
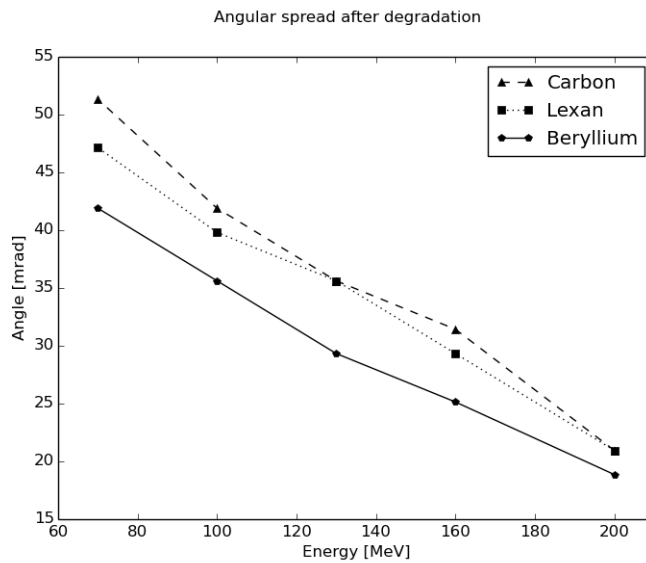

Figure 4.6: HWHM of the angular spread for the proton beam after the degrader for an uncollimated beam. Initial proton energy: 250 MeV.
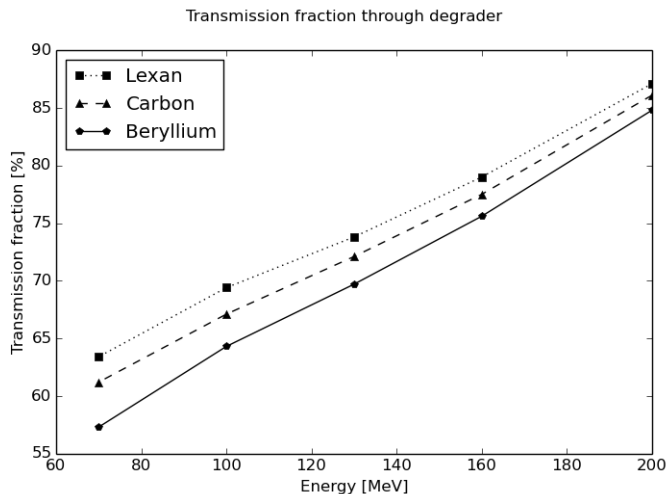
Figure 4.7: Transmission fraction of the incoming protons after passing the degrader for an uncollimated beam. Initial proton energy: 250 MeV.

grader has the lowest transmission fraction and lexan the highest.

The fraction of protons that exits the degrader within the allowed momentum spread, in this case 1.2% of the mean energy, is the theoretical maximum transmission fraction. This is presented in figure 4.8. As the momentum spread is quite similar for all materials, these differences mainly reflects the differences in total transmission.

The fraction of protons transmitted through the degrader with a smaller angular spread than 12 mrad is presented in figure 4.9. The figure shows that the fraction of protons is strongly decreasing as the beam is degraded more, due to more coloumb scattering increasing the angular spread of more protons. This shows that even though the beryllium degrader has the lowest transmission fraction, the scattering is so much lower that there are more protons coming through the degrader with an acceptable angular spread for beryllium degraders than for lexan and carbon.
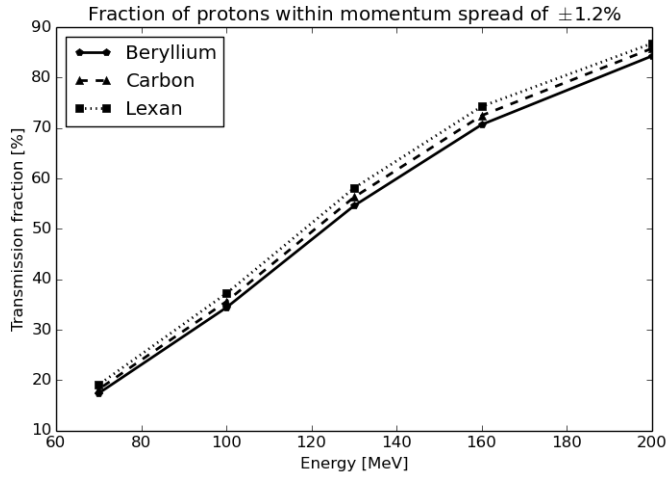
Figure 4.8: Fraction of protons that exits the degrader with a momentum spread of less than 1.2 % for an uncollimated beam. Initial proton energy: 250 MeV.
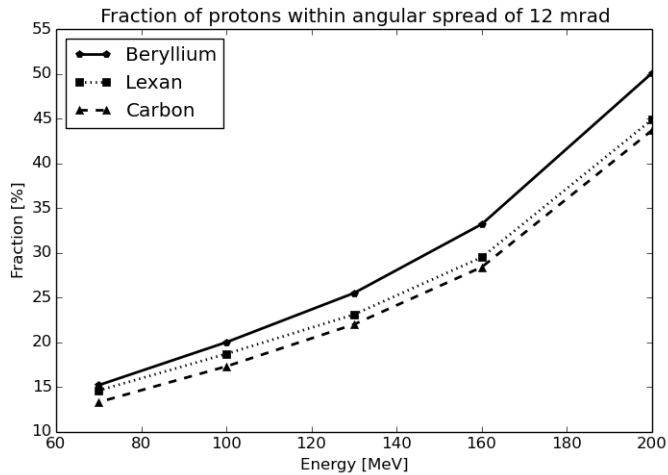

Figure 4.9: Fraction of protons in the uncollimated degraded beam with an angular spread less than 12 mrad. Initial proton energy: 250 MeV.
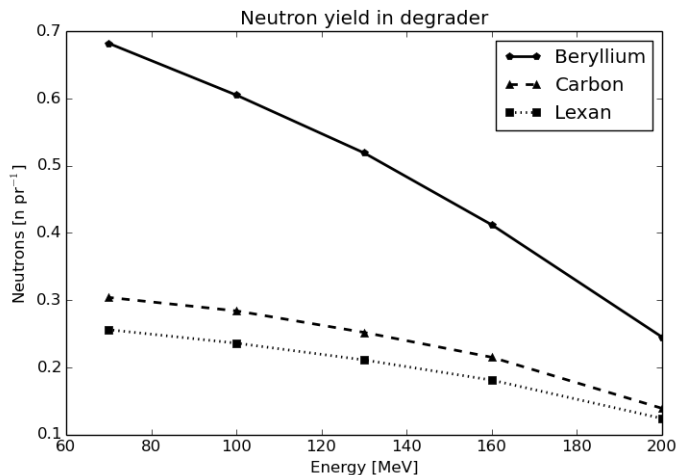
Figure 4.10: Neutron yield per proton in the primary beam for an uncollimated beam. Initial proton energy: 250 MeV.

4.1.6 Neutron yield

The number of neutrons generated in the degrader is shown in figure 4.10. There is generated more than twice as many neutrons in the beryllium degrader than the degraders made of carbon or lexan per primary proton.

The amount of neutrons should however be compared per proton in the degraded beam, because a treatment dose is depending on the protons actually reaching the patient. This is presented in figure 4.11. The same trend is apparent here. The beryllium degrader generates ca. twice as many neutrons as the other degrader materials.

4.1.7 Photon yield

The number of photons generated in the degrader is shown in figure 4.12. While the photon yield for carbon and lexan degraders is increasing as
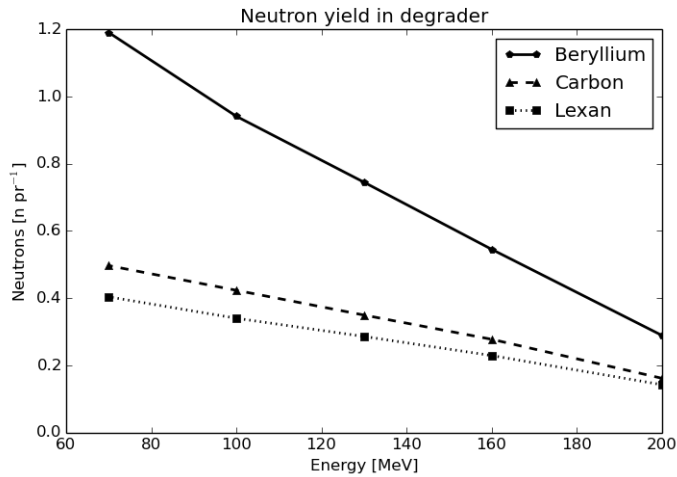
Figure 4.11: Neutron yield per proton in the uncollimated degraded beam. Initial proton energy: 250 MeV.

the beam is degraded more, the photon yield for the beryllium degrader almost constant. The amount of photons generated per proton in the degraded beam, as shown in figure 4.13, is almost constant for a beryllium degrader, while it is linearly increasing for carbon and lexan degraders. The photon yield for carbon and lexan degraders are a factor 1.5 - 3 higher than for a beryllium degrader.
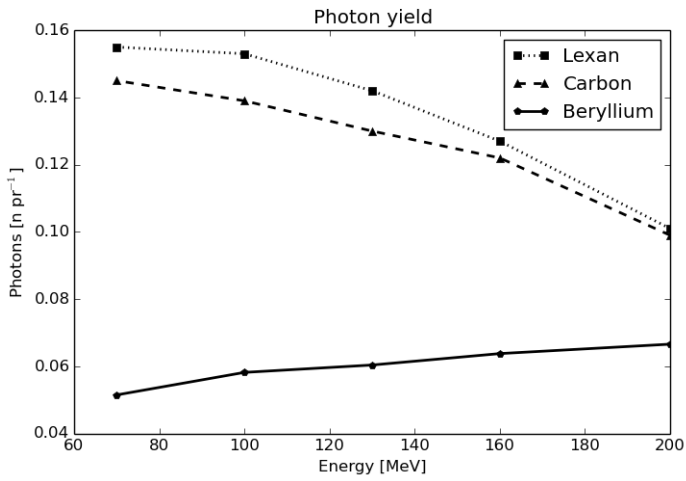
Figure 4.12: The figure shows the photon yield per proton in the primary beam for an uncollimated beam. Initial proton energy: 250 MeV.
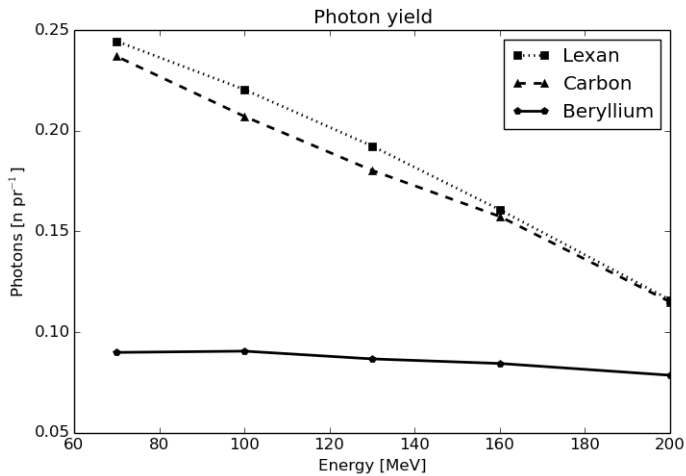

Figure 4.13: The figure shows the photon yield per proton in the uncollimated degraded beam. Initial proton energy: 250 MeV.
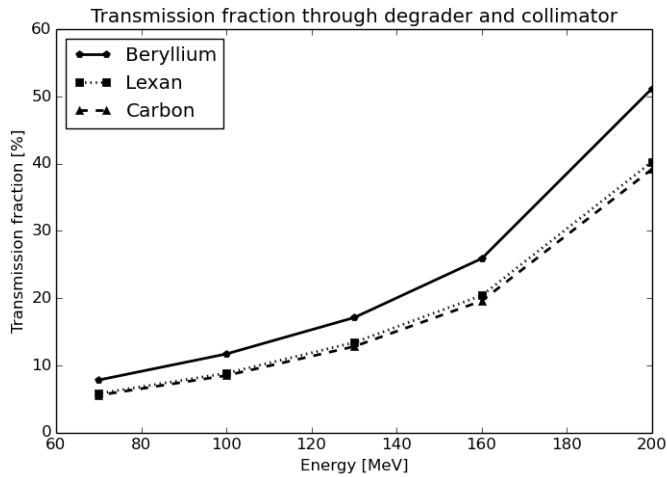
Figure 4.14: The figure shows the transmission fraction in the degrader and collimator for the collimated beam. Initial proton energy: 250 MeV.

4.2 Collimated beam

4.2.1 Transmission fraction

The transmission fraction through the degrader and collimator for the collimated beam is shown in figure 4.14. The transmission fractions for carbon and lexan degraders are approximately equal. The transmission fraction varies from 40-50% at 200 MeV to below 10% at 70 MeV.

Taking into account the desired momentum interval, the transmission fraction is further reduced, as shown in figure 4.15. The transmission fraction is between 20-30% at 200 MeV and is decreasing down to around 2% at 70 MeV. The beryllium degrader gives 27% and 30% higher transmission fraction at 200 MeV than for the lexan and carbon degraders, respectively. The difference is increasing with decreasing beam energy to 36% and 43% at 70 MeV.
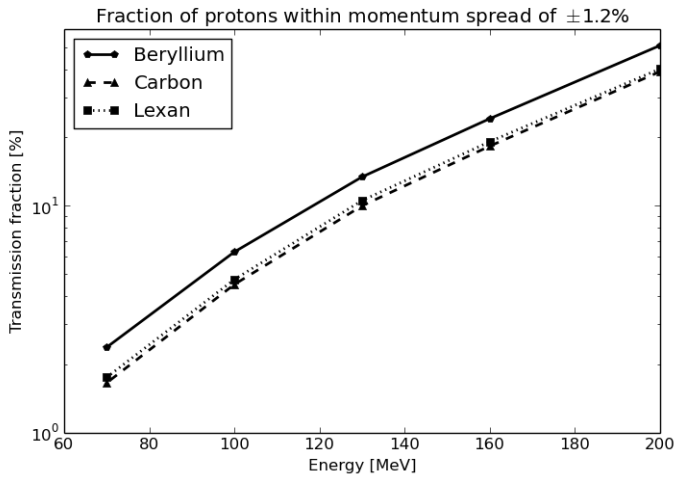
Figure 4.15: The figure shows the fraction of protons that leaves the de-grader and collimator with a momentum spread within 1.2 %. The log-arithmic y-axis makes it easier to see the relative difference between the different degrader materials for the lowest beam energies. Initial proton energy: 250 MeV.

4.2.2   Angular spread

The HWHM of the angular spread of the collimated degraded beam is shown in figure 4.16. For lexan the HWHM is slightly increasing for more degraded beams. For the other degrader materials, the HWHM is approx-imately constant, with a possible increase for more degraded beams.

4.2.3   Neutron yield

The neutron yield per primary proton for the collimated beam is pre-sented in figure 4.17. The neutron yield is increasing the more the beam is degraded for beryllium degrader, while it is decreasing for carbon and lexan degraders. The neutron yield per proton in the collimated degraded beam, however, turns out to be quite similar for all degrader materials as
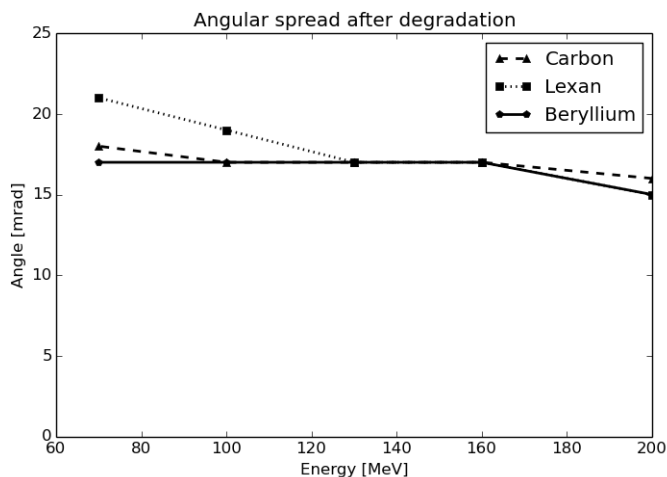
Figure 4.16: The figure shows the HWHM of the angular spread of the collimated degraded beam. Initial proton energy: 250 MeV.

shown in figure 4.18. The decreasing transmission fraction for more degraded beams leads to an increase in neutron yield for lower energies. However, the neutron yield in the beryllium degrader for lower energies is higher than for carbon or lexan. For 70 MeV the amount of neutrons generated is increased with 50 % compared to a carbon degrader, and with 82 % compared to a lexan degrader. In figure 4.19 and 4.20 we can see the neutron fluence for a 200 MeV collimated beam. From this we can see that the main neutron source in the carbon system is the collimator, while the degrader plays a much more important role in the degrader system. This explains the developement of neutron yield for lower energies. The increase in neutrons generated in the degrader is bigger than the decrease in neutrons generated in the collimator for the beryllium degrader. For the carbon and lexan degraders the decrease in neutrons generated in the collimator is bigger than the increase in neutrons generated in the degrader for lower energies. This leads to the reduction in

Figure 4.17: Neutron yield for the collimated beam per proton in the primary beam. Initial proton energy: 250 MeV.

neutron yield per primary proton for lexan and carbon degraders.

4.2.4   Photon yield

The photon yield per primary proton is presented in figure 4.21. The photon yield per primary proton is reduced when the degraded beam energy is reduced. However, as the transmission fraction is reduced for lower energies, the photon yield per proton in the collimated degraded beam is increasing for lower energies, as shown in figure 4.22. The photon yield for the carbon and the lexan degrader is quite similar, while the photon yield is reduced with 40% to 56% for beryllium, with increasing difference for lower beam energies.
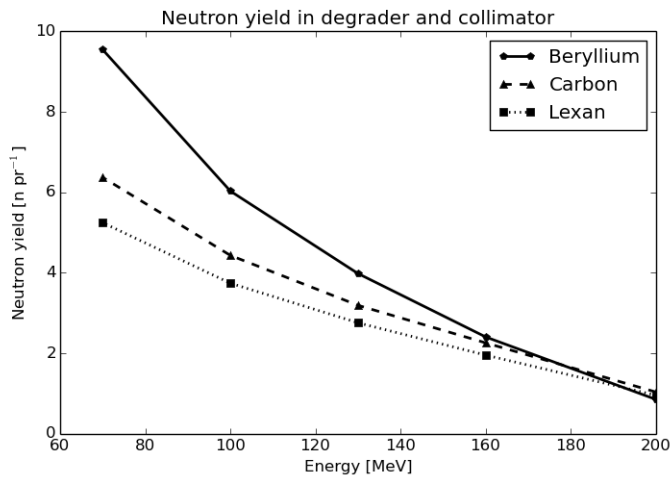
Figure 4.18: Neutron yield per proton in the collimated degraded beam. Initial proton energy: 250 MeV.
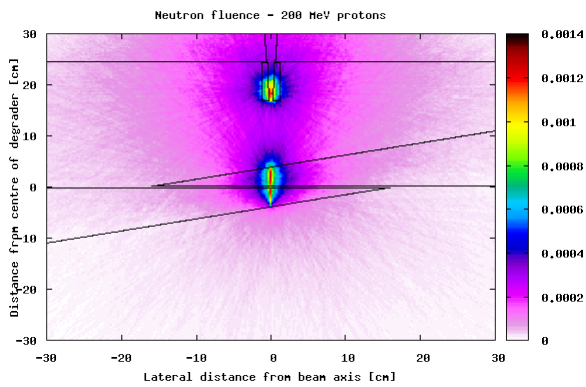
Figure 4.19: Neutron fluence per primary proton for a collimated beam degraded to 200 MeV by a beryllium degrader.
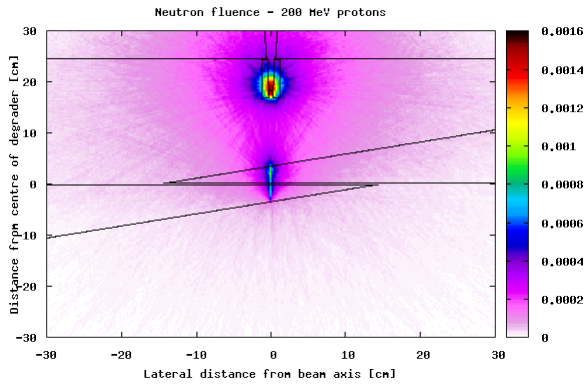
Figure 4.20: Neutron fluence per proton for a collimated beam degraded to 200 MeV by a carbon degrader.
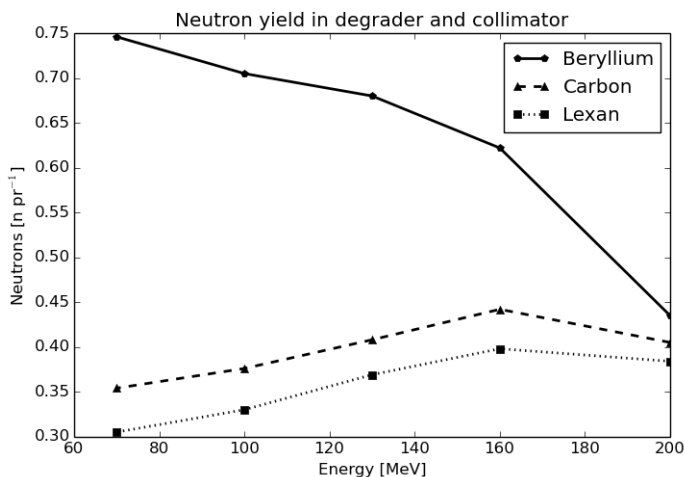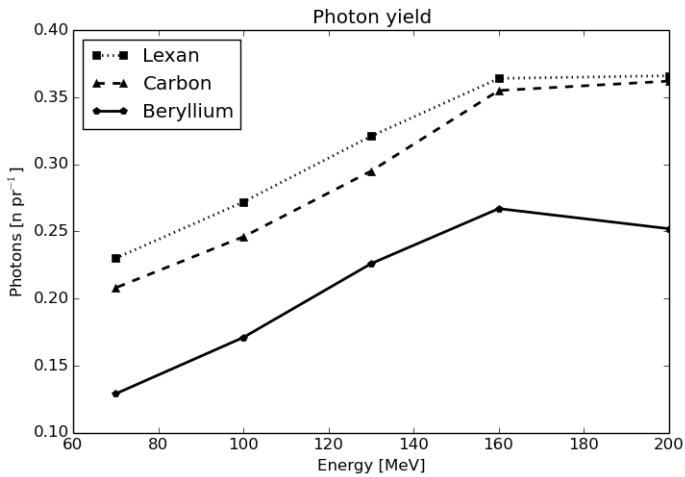

Figure 4.21: Photon yield for the collimated beam per proton in the primary beam. Initial proton energy: 250 MeV.
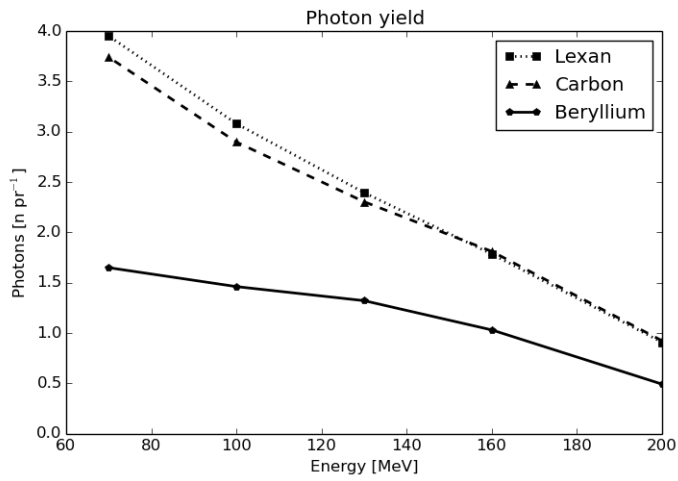
Figure 4.22: Photon yield per proton in the collimated degraded beam. Initial proton energy: 250 MeV.

Chapter 5

Discussion

5.1 Momentum spread

As presented in figure 4.3, the momentum spread of the proton beam after degradation is almost identical for all studied materials. As a consequence, there is no difference in the fraction of particles that will be filtered in the momentum analyzer or the generation of secondary particles in the momentum analyzer. Even though there are differences in the thickness of the degraders, this does not influence the momentum spread of the beam. These simulations indicates that the momentum spread is independent of the degrader material. This corresponds well with similar research done by Hsi et al. which states that the momentum spreads for beryllium, carbon and water are almost identical [24] for a proton beam degraded from 250 MeV.

5.2   Distal penumbra

The distal penumbra for this proton beam without any momentum an-
alyzer is constant for all energies. The protons are stopped during reac-
tions in the degrader and the water phantom. Whether most of the stop-
ping happens in the degrader or the water phantom do not influence the
distal penumbra, which is caused by range straggling. This corresponds
well with research on compact centre with no momentum analyzing sys-
tem and initial proton energy on 250 MeV, which concludes with a dis-
tal penumbra at arouond 6 mm for all energies [25]. This indicates that
the momentum spread for water also is about the same as the actual de-
grader materials.

5.3   Angular spread

The scoring of angular spread that has been done in this simulations has
some inaccuracies. The fluence has been scored for the area between the
degrader ESS and the phantom, but the results do not actually say any-
thing about the actual angle of the velocity of the protons. The angular
distribution that is presented in figure 4.5 is the proton fluence in a area
of 20 cm before the water phantom. The angle is relative to origo. The
multiple scattering in the degrader may lead to different pathways. The
measured angular spread turned out to be constant during the region
of interest. Even though there are some uncertainties around the excact
values of the angular spread, the qualitative differences between the dif-
ferent energies and materials do still give us useful information about the
spread for different materials. Beryllium is without doubt scattering less
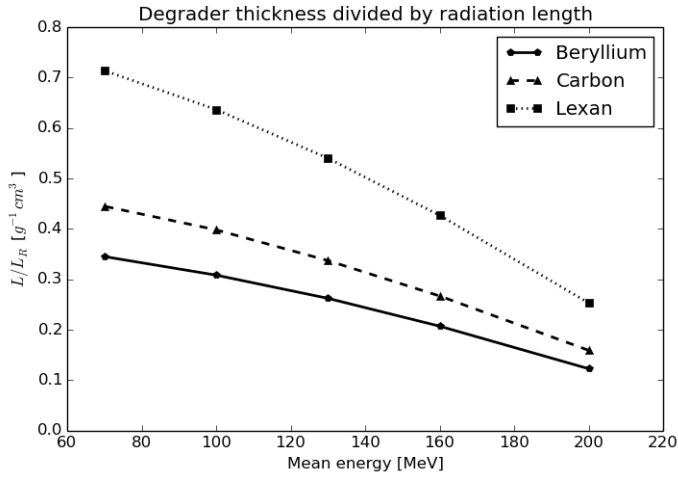
Figure 5.1: Degrader thickness divided by radiation length for the different beam energies.

than carbon and lexan. The USRBIN card, however, showed not to be an ideal tool for scoring the angular distribution. The maximum number of bins was limited to 3000, which gives a resolution at ca 2 mrad.

Highland's equation(Equation 2.2) says that the angular spread depends on the relation between material thickness, L, and the radiation length, L_R. This relation is shown in figure 5.1. Here we can see that the berylium degrader gives the lowest L/L_R ratio, but carbon gives a much lower ratio than lexan. This should imply that a lexan degrader should give a higher angular spread. According to these results, carbon and lexan degraders gives approximately the same angular spread.

5.4 Transmission fraction

The transmission fraction through the degrader is affected by the multiple scattering and nuclear interactions in the degrader. While Beryllium

has the highest beam loss due to nuclear interactions, the reduced multiple scattering leads to a higher transmission fraction in the end. Especially in cases where it is important to maintain a high doserate even at low energies, the difference in transmission fraction might be an important parameter. Depending on the properties of the momentum slit, the transmission fraction may be even lower than what is presented here.

5.5   Neutron yield

The neutron yield for the lowest energies was highest in the beryllium degrader. For higher energies the neutron yield was at same level as for the carbon and lexan degrader due to the increased neutron yield in the collimator. However, for lower energies the increased neutron yield in the degrader and the reduced neutron yield in the collimator, due to reduced proton energy, led to that the neutron yield in the beryllium degrader setup increased compared to the other setups. Part of the reason for the increased neutron yield in beryllium may be that beryllium has a high cross section for generation of new neutrons (n,2n) [4]. The increased neutron yield for beryllium degraders leads to that extra precautions need to be taken in order to keep the environment safe for harmful neutron radiation. A beryllium degrader is therefore not a good choice for a compact proton facility, with a degrader close to the treatment room [26]. When the degrader is placed well shielded far away from the treatment room, the problem with neutron radiation is minimized. In addition to the potential dangerous neutron radiation, these neutrons also lead to increased radioactive activation of the elements surrounding

the beam line.

5.6 Initial energy

These simulations have been done with an initial energy of 250 MeV for the proton beam. If the initial energy had been reduced to 230 MeV, or lower, there might have been some differences in the neutron yield results. According to Anferov et al. [7] the neutron production cross section for 200 MeV protons is lower for beryllium than for carbon.

5.7 Possible inconveniences with beryllium

There are some concerns about that beryllium is brittle and toxic [4], and that this will give some practical complications concerning maintenance of the beam line. Beryllium is indeed a toxic metal that is specially harmful by inhalation [27], but the effect of this not particulary well known. According to Laddie Derenchuk at ProNova Solutions, the beryllium degrader they use there is coated with beryllium oxide, which is non-toxic, and the degrader is out of possible contact by anyone other than service personnel [28].

5.8 Suggestions for further work

The simulations done in this work do not include focusing quadrupole magnets. Including of quadrupole magnets in the input will give a more realistic beamline. Properties of the focusing of the beam could also af-

fect the results of the angular spread after degradation [9]. Focusing mag-
nets play an important role in reducing the beam loss and are therefore
crucial for a realistic simulation of the energy selection system. A more
thorougly study of the energy selection system should also include the
momentum analyzer. The momentum slit, which stops protons with un-
desired momentum, will give rise to neutron yield [5]. The neutron con-
tribution from the momentum slit will increase for lower energies, as the
momentum spread increases. Another way to improve the simulations is
to implement an entire SOBP that provides a homogenous dose to a tar-
get volume in a water phantom. This way it will be possible to measure
the actual generated neutron yield for a specific dose fraction. In order to
do this, it is important to have a setup with both quadrupole magnets and
momentum analyzer, which can be a realistic therapeutic proton beam.
By doing this, the entire neutron yield from the ESS for a proton ther-
apy fraction can be simulated, and thereby also better estimations of the
neutron dose.

Chapter 6

Conclusion

The influence of the degrader material for a 250 MeV therapeutical proton beam has been investigated. The momentum spread was not affected by the degrader material. The total transmission fraction is decreasing with decreasing beam energy from around 20-30% at 200 MeV to around 2% at 70 MeV. It has been shown that a beryllium degrader reduces the angular spread compared to carbon and lexan. Hence, a beryllium degrader will increase the transmission fraction with 27-43 % compared to a carbon degrader or lexan degrader, with biggest difference at low energies. The neutron yield in a beryllium degrader is significantly higher than in a carbon degrader or lexan degrader, and will increase the amount of neutrons generated with up to 50 % compared to a carbon degrader and up to as much as 82 % compared to a lexan degrader. These results tells that beryllium is a well suited material if it is important to maintain a high transmission fraction at low energies and reduce the angular spread of the beam. But as beryllium increases the neutron yield, it is especially important that it is possible to make sure that the degrader is

sufficiently shielded. Based on this results beryllium does not look like a attractive choice for a compact center, with a degrader close to the treatment room. A natural next step for further work will be to implement qudrupole magnets to focus the beam and a momentum analyzer to get a more monoenergetic beam. This will take into account all the important elements in the ESS. It would also be of interest to deliver a full SOBP to the water phantom and thereby measure the total neutron yield for a 2 Gy fraction to a target volume in the water phantom.

Appendix A

Input File

An example of a input file. This is the input file for the 200 MeV beryllium
degraded collimated beam:

TITLE

* Set the defaults for precision simulations
DEFAULTS
PRECISIO
* Define the beam characteristics
BEAM   −0.25   −0.0023   −0.25   −0.25
PROTON
* Define the beam position
BEAMPOS   −20.   0.0   0.0   1.
GEOBEGIN
COMBNAME
     0   0
* Black body

SPH blkbody   0.0 0.0 0.0 1000.0

∗ Water sphere

SPH void   0.0 0.0 0.0 400.0

∗ Vacuum sphere

SPH sphere   0.0 0.0 0.0 65.0

∗ First wedge

WED wedge1   −0.2 −10.0 −22.1 0.0 0.0 70.0 −16.471 0.0 0.0 0.0 20.

∗ Second wedge

WED wedge2   0.2 −10.0 22.1 0.0 0.0 −70.0 16.471 0.0 0.0 0.0 20.0

∗ Collimator

RCC coll   16.871 0.0 0.0 7.5 0.0 0.0 1.3

∗ Collimator hole

TRC chol   16.771 0.0 0.0 7.7 0.0 0.0 0.35 0.514

∗ Collimator

RCC coll1   24.6 0.0 0.0 12.5 0.0 0.0 30.0

∗ Collimator hole

TRC chol1   24.5 0.0 0.0 12.7 0.0 0.0 0.65 1.25

∗ Water phantom

RPP phantom   70. 100. −5. 5. −5. 5.

END

∗ Black hole

BLKBODY   5 +blkbody −void

∗ Water sphere to score dose

VOID   5 +void −sphere −phantom

∗ Vacuum sphere around the degrader

SPHERE   5 +sphere −wedge1 −wedge2 −(coll−chol) −(coll1 −chol1

```
* First wedge
WEDGE1          5 +wedge1
* Second wedge
WEDGE2          5 +wedge2
* Second wedge
COLL            5 +coll -chol
* Second wedge
COLL1           5 +coll1 -chol1
* Second wedge
PHANTOM         5 +phantom
END
GEOEND
* ..+....1....+....2....+....3....+....4....+....5....+....6....+...
ASSIGNMA    BLCKHOLE    BLKBODY
ASSIGNMA     VACUUM       VOID
ASSIGNMA     VACUUM     SPHERE
ASSIGNMA    BERYLLIU    WEDGE1
ASSIGNMA    BERYLLIU    WEDGE2
ASSIGNMA     COPPER       COLL
ASSIGNMA     CARBON      COLL1
ASSIGNMA      WATER    PHANTOM
* Energy spectrum after energy modulation.
* NB: Correct energy interval.
USRBDX          101.    PROTON         -29.       VOID    PHANTOM
Proton
```

USRBDX   0.08   0.06   200.

&

* Energy spectrum for neutrons generated in degrader.

USRBDX   99.   NEUTRON   −30.   SPHERE   VOID

Neutron

USRBDX   0.25   1E−14   300.

&

* Energy spectrum for photons generated in degrader.

USRBDX   99.   PHOTON   −31.   SPHERE   VOID

Photon

USRBDX   0.25   1E−8   300.

&

* Beam emmitance after energy modulation.

USRBIN   11.   PROTON   −22.   50.

2.Angular

USRBIN   30.   −2.   1.   2999.

1. &

* Distal dose distribution. (Bragg peak & Distal penumbra)

USRBIN   10.   DOSE   −23.   80.

10.   10.DistDose

USRBIN   70.   −10.   −10.   1000.

1.   1. &

* Visual of beam

*USRBIN   10.   PROTON   −32.   100.

1.   5.Visual

```
*USRBIN              0.0          −1.          −5.          1000.
1.        100. &
* Set the random number seed
RANDOMIZ             1.0          1.
* Set the number of primary histories to be simulated in the run
START               1E5
STOP
```

Bibliography

[1] W. C. Röntgen, "On a New Kind of Rays," *Science*, vol. 3, pp. 227–231, Feb. 1896.

[2] R. R. Wilson, "Radiological Use of Fast Protons," *Radiology*, vol. 47, pp. 487–491, Nov. 1946.

[3] J. Y. Chang, X. Zhang, X. Wang, Y. Kang, B. Riley, S. Bilton, R. Mohan, R. Komaki, and J. D. Cox, "Significant reduction of normal tissue dose by proton radiotherapy compared with three-dimensional conformal or intensity-modulated radiation therapy in Stage I or Stage III non–small-cell lung cancer," *International Journal of Radiation Oncology*Biology*Physics*, vol. 65, pp. 1087–1096, July 2006.

[4] M. J. v. Goethem, R. v. d. Meer, H. W. Reist, and J. M. Schippers, "Geant4 simulations of proton beam transport through a carbon or beryllium degrader and following a beam line," *Physics in Medicine and Biology*, vol. 54, p. 5831, Oct. 2009.

[5] H. Paganetti, *Proton Therapy Physics.* Series in Medical Physics and Biomedical Engineering, Boca Raton, FL: CRC Press, 2012.

[6] M. Awschalom, "Radiation Shielding for 250-MeV Protons," 1987.

[7] V. A. Anferov, M. S. Ball, J. C. Collins, and V. P. Derenchuk, "Indiana University cyclotron operation for proton therapy facility," in *Proceedings of the 18th International Conference on Cyclotrons and their Applications*, pp. 1–5, 2007.

[8] H.-J. Borchert, M. Mayr, R. A. Schneider, M. R. Arnold, D. E. Geismar, M. Wilms, L. Wisser, and M. Herbst, "Proton therapy with spot scanning: the Rinecker Proton Therapy Center in Munich. Part 2: Technical & physical aspects," *NOWOTWORY*, vol. 58, no. 2, pp. 62e–70e, 2008.

[9] V. Anferov, "Energy degrader optimization for medical beam lines," *Nuclear Instruments and Methods in Physics Research Section A: Accelerators, Spectrometers, Detectors and Associated Equipment*, vol. 496, no. 1, pp. 222–227, 2003.

[10] A. Ferrari, P. R. Sala, A. Fasso, and J. Ranft, "FLUKA: A multi-particle transport code (Program version 2005)," tech. rep., 2005.

[11] W. R. Leo, *Techniques for Nuclear and Particle Physics Experiments: A How-to Approach.* Springer Science & Business Media, Dec. 2012.

[12] S. Tavernier, "Interactions of particles in matter," in *Experimental Techniques in Nuclear and Particle Physics*, pp. 23–53, Springer, 2010.

[13] T. Hayashi, K. Tobita, Y. Nakamori, and S. Orimo, "Advanced neutron shielding material using zirconium borohydride and zirconium hydride," *Journal of Nuclear Materials*, vol. 386–388, pp. 119–121, Apr. 2009.

[14] J. Lilley, *Nuclear Physics*. Wiley, 2001.

[15] T. Bortfeld, "An analytical approximation of the Bragg curve for therapeutic proton beams," *Medical Physics*, vol. 24, pp. 2024–2033, Dec. 1997.

[16] H. Paganetti, "Range uncertainties in proton therapy and the role of Monte Carlo simulations," *Physics in Medicine and Biology*, vol. 57, p. R99, June 2012.

[17] W. Wieszczycka and W. Scharf, *Proton Radiotherapy Accelerators*. World Scientific, Jan. 2001.

[18] M. Durante and S. Galès, *Nuclear Physics for Medicine - Hadrontherapy*. Nuclear Physics European Collaaboration Committee (NuPECC), 2014.

[19] S. A. Kostromin and E. M. Syresin, "Trends in accelerator technology for hadron therapy," *Physics of Particles and Nuclei Letters*, vol. 10, pp. 833–853, Jan. 2014.

[20] J. M. Schippers, J. Duppich, G. Goitein, M. Jermann, A. Lomax, E. Pedroni, H. Reist, B. Timmermann, and J. Verweij, "The use of protons in cancer therapy at PSI and related instrumentation," *Journal of Physics: Conference Series*, vol. 41, p. 61, May 2006.

[21] V. Vlachoudis and others, "FLAIR: a powerful but user friendly graphical interface for FLUKA," in *Proc. Int. Conf. on Mathematics, Computational Methods & Reactor Physics (M&C 2009), Saratoga Springs, New York*, 2009.

[22] K. Parodi, S. Brons, H. Paganetti, F. Sommerer, F. Cerutti, A. Ferrari, and A. Mairani, "The FLUKA code for application of Monte Carlo methods to promote high precision ion beam therapy," 2010.

[23] F. Stichelbaut and Y. Jongen, "Properties of an energy degrader for light ions," 2014.

[24] W. C. Hsi, M. F. Moyers, D. Nichiporov, V. Anferov, M. Wolanski, C. E. Allgower, J. B. Farr, A. E. Mascia, and A. N. Schreuder, "Energy spectrum control for modulated proton beams," *Medical Physics*, vol. 36, pp. 2297–2308, June 2009.

[25] C. Bloch, P. M. Hill, K. L. Chen, A. Saito, and E. E. Klein, "Startup of the Kling Center for proton therapy," in *Application of Accelerators in Research and Industry: 22nd International Conference*, 2012.

[26] C.-M. C. Ma and T. Lomax, *Proton and Carbon Ion Therapy.* CRC Press, Oct. 2012.

[27] M. Jakubowski and C. PałczyŃski, "Chapter 30 - Beryllium," in *Handbook on the Toxicology of Metals (Fourth Edition)* (G. F. N. A. F. Nordberg, ed.), pp. 635–653, San Diego: Academic Press, 2015.

[28] V. Derenchuk, "Personal communication by e-mail," July 2015.